Eco-friendly PVA-LYS fibers for gold nanoparticle recovery from water and their catalytic performance

This version of the article has been accepted for publication, after peer review (when applicable) and is subject to Springer Nature's AM terms of use, but is not the Version of Record and does not reflect post-acceptance improvements, or any corrections. The Version of Record is available online at: https://doi.org/10.1007/s11356-023-26912-7

Eco-friendly PVA-LYS fibers for gold nanoparticles recovery from water and their catalytic performance

Eya Ben Khalifa[a], Claudio Cecone[a], Pierangiola Bracco[a], Mery Malandrino[a], Maria Cristina Paganini[a], Giuliana Magnacca[a]

[a] Department of Chemistry and NIS Interdepartmental Centre, Torino University, Via P. Giuria 7, 10125 Torino, Italy

Corresponding Author: Claudio Cecone, Email: claudio.cecone@unito.it, Tel. +390116707558

Abstract

In this work, we grafted lysine on PVA electrospun fibers, using a green preparation technique. The resulting fiber mats were proposed for gold nanoparticles (AuNPs) removal from water. The efficiency of three fibers with different lysine amounts (10, 20 and 30%) was investigated. The incorporation of amino groups in PVA fibers was firstly proved by FTIR, SEM and elemental analysis, confirming the presence of lysine. Among the three different fibers, PVA-LYS 30% has shown the best removal efficiency, reaching 65%, at pH equal to 5. Adsorption isotherms were studied and showed that the Langmuir model is the best model fitting our experimental results, with a maximum adsorption capacity of 20.1 mg g^{-1}. Metal-ligand interactions and electrostatic attraction between protonated amino groups of lysine on the fibers and negatively charged, citrate capped, AuNPs are the main proposed mechanisms for AuNPs adsorption on the fibers. Sustainability of AuNPs adsorbed on these fibers has been checked through their reuse as catalyst for the reduction of 4-nitrophenol to 4-aminophenol. The process was completed within 60 min and their reusability showed more than 99% efficiency after 5 reduction cycles. Our results prove that green PVA-LYS fibers

can extract nanoparticles from water, as low cost effective and eco-friendly adsorbent, and contribute to the promotion of a circular economy approach, through their reuse as catalyst in the reduction of pollutants.

Keywords: Electrospinning, Polyvinyl alcohol, Lysine, Surface modification, Green crosslinking, Nanoparticles

Abbreviations

PVA: Polyvinyl Alcohol

LYS: Lysine

AuNPs: Gold nanoparticles

FTIR: Fourier Transform Infrared Red Spectroscopy

CAGR: Compound Annual Growth Rate

CIRC: International Center of Research on Cancer

SEM: Scanning Electron Microscopy

TEM: Transmission Electron microscopy

TGA: Thermogravimetric Analysis

PVA-CA: Polyvinyl Alcohol -Citric Acid fibers

ATR: Attenuated Total Reflectance

pH_{pzc}: pH of zero charge

ICP-OES: Inductively Coupled Plasma - Optical Emission Spectroscopy

U.S.: United States

1. Introduction

Metallic nanoparticles have received great interest due to their unique optical (Zhang et al. 2013), electrical and magnetic (Rudakov et al. 2019) properties, their high surface to volume ratio, small size and peculiar, adjustable shapes (Thakur et al. 2022). These properties are interesting in numerous applications, including cell imaging (Karmakar et al. 2019), sensors

(Montes-Garcı et al. 2021), and sunlight energy conversion (Zhang et al. 2022). They are considered as promising tools for light and magnetic based tumor visualization and guided drug delivery (Kuchur et al. 2020). Gold nanoparticles (AuNPs) have been used in cancer remediation in recent years, because of their facile synthesis and surface modification, their unique surface plasmon resonance, as well as excellent biocompatibility (Huang and El-Sayed 2010). Applications related to plasmon absorption and scattering of AuNPs are impressively numerous, ranging from sensing and photothermal effects, to cell imaging (Amendola et al. 2017). Despite the unique advantages of metallic NPs, their adverse effects, related to short and long term toxicity are a critical issue. Different studies have been conducted to explore the dark side of nanotechnology (Grieger et al. 2019; Haase et al. 2012; Hochella et al. 2019). The nanotoxicity includes cytotoxicity, genotoxicity, production of reactive oxygen species (ROS), oxidative stress and inflammation, modulation of cell signaling and cancer (Manuja et al. 2021). The global market for nanotechnology is expected to grow from $2.0 billion in 2018 to $2.1 billion by 2023, at a compound annual growth rate (CAGR) of 19.4% (BBC research reports 2021). This huge production of nanomaterials will increase their release in the environment (soil, water, and atmosphere) and cause a higher risk to the ecosystem and human health (Du et al. 2020; Mao et al. 2018). Therefore, progress in reducing nanoparticles release of and/or developing efficient removal techniques is urgently needed. Research studies on their removal from water are at the first stage and limited investigations are available in the literature. The efficiency of porous melamine-formaldehyde resin (Li et al. 2021), functionalized carbon spheres (Kumar et al. 2014), amine-functionalized block copolymers (Querchi et al. 2014) and cellulose based nanofibers (Mahanta et al. 2012) has been evaluated to reduce the levels of AuNPs in water. The preparation of the previously mentioned adsorbents was usually done using toxic chemicals like glutaraldehyde, formaldehyde, and tetrahydrofuran. In contrast, this work focuses on the

use of green and ecofriendly crosslinking agent to produce electrospun fibers as AuNPs adsorbents from aqueous solutions.

Green electrospun fibers have shown excellent efficiency in water remediation. Picón et al. 2022 reported a novel immobilized L-cysteine on PVA nanofibers to remove arsenic from water. PAN fibers have been used by Alarifi et al. 2020 as a filtration membrane to remove pollutants from municipal wastewater. Wang et al. 2022 prepared an eco-friendly calcium crosslinked alginate electrospun nanofibers with high adsorption efficiency of copper, reaching 285.5 mg g^{-1}. Moreover, Elkady et al. 2020 fabricated PVA / alginate / chitosan nanofibers for phenol decontamination. Electrospinning is a promising technique, getting an increasing interest due to its simplicity, efficiency, low cost, and easy scalability (Zhang et al. 2022; Omer et al. 2021). This technique is based on flowing a polymer solution through a syringe, while an electrical field is applied to the polymer droplet. Once the electrostatic repulsion of the charged polymer liquid becomes higher than the surface tension, a conical shape, known as Taylor's cone, forms and the jet initiation starts from the cone tip. The produced fibers are deposited on a metallic collector (Fig. 1). Polyvinyl alcohol (PVA) is a synthetic polymer, characterized by its non-toxicity, biodegradability, low cost, biocompatibility, and good mechanical strength (Park et al. 2017; Zhan et al. 2021). It has been widely used as blending polymer in electrospinning for different applications: tissue engineering scaffolds (Teixeira et al. 2019), food packaging and water treatment (Zhang et al. 2019; Zhang et al. 2020). PVA is water-soluble thanks to the presence of hydroxyl groups (Thong et al. 2016), then PVA nanofibers can be easily obtained from the electrospinning of aqueous solutions. On the other hand, an appropriate crosslinking step after electrospinning can guarantee the stability of the fibers in an aqueous environment. Different chemical agents such as glutaraldehyde (Mansur et al. 2008), glyoxal (Zhang et al. 2010), formaldehyde and methanol (Franco et al. 2012) were previously used as cross-linkers. However, these agents

104 are highly dangerous for human health and classified as carcinogen by the CIRC (ANSES,
105 2021). As an alternative, citric acid was added to the polymer blending, as a green and non-
106 toxic crosslinker, in this work (Cecone et al. 2022). Lysine (2,6-diaminohexanoic acid) is
107 one of the essential amino acids, containing two amino groups and α-carboxylic acid group
108 (Stagi et al. 2022). The presence of these functional groups offers different advantages when
109 lysine is loaded on PVA electrospun fibers: the amide bond formation between carboxylic
110 groups of citric acid and amino groups of lysine enhances the grafting of lysine to the
111 polymer substrate, while the reactivity of the residual amino groups can be exploited as
112 active sites for metallic nanoparticles adsorption, thanks to their ability to bind to the NPs
113 (Lapenna et al. 2020; Liguori et al. 2019).
114

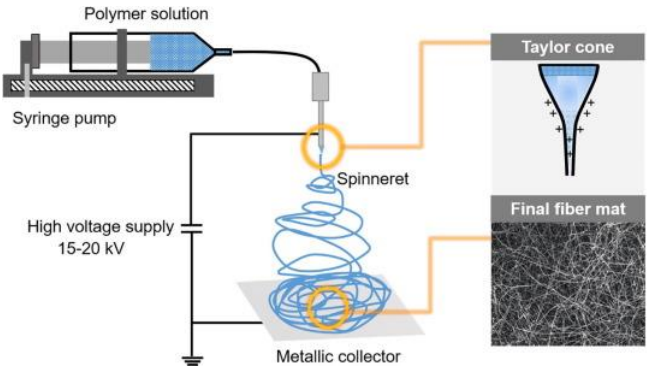

115
116 **Fig. 1** Electrospinning set up (Wen et al. 2021)

117 This study investigates the use of lysine grafted PVA fibers, as green adsorbent of AuNPs
118 from water. To test the efficiency of these fibers, three different amounts of lysine were
119 added to the PVA polymer mixture. The produced fibers were characterized by
120 scanning electron microscopy (SEM), Fourier Transform InfraRed spectroscopy (FTIR),
121 thermogravimetric analysis (TGA), elemental analysis, and pH of zero charge. Batch
122 adsorption experiments were conducted in a pH range of 5 to 9, with an amount of adsorbent
123 from 5 to 20 mg and at two concentrations of AuNPs. Adsorption kinetics and isotherms
124 were studied, and an adsorption mechanism has been proposed. Finally, the catalytic

performance of the recovered AuNPs was evaluated through the reduction of 4-nitrophenol to 4-aminophenol and a reusability test was carried out to check the recyclability of these fibers after AuNPs adsorption.

2. Materials and Methods

2.1. Materials

Polyvinyl alcohol (PVA) 99 % hydrolyzed, with an average molecular weight of 89000 - 98000 Da, hydrogen tetrachloroaurate trihydrate ($HAuCl_4$. $3H_2O$), trisodium citrate ($Na_3C_6H_5O_7$), sodium hydroxide (NaOH), hydrochloric acid (HCl), Lysine (Lys), sodium borohydride ($NaBH_4$), nitric acid (HNO_3) and hydrogen peroxide (H_2O_2) were purchased from Sigma Aldrich. 4-Nitrophenol (4-NP) was supplied by Merck. All chemicals were analytical grade. Deionized water was used to prepare the solutions.

2.2. AuNPs synthesis

AuNPs were prepared using the trisodium citrate reduction method according to the procedure proposed by Li. et al. (2011). Briefly, 2 mL of chloroauric acid solution (25 mM) were introduced into a flask, then 6.6 mL of NaOH (20 mmol L^{-1}) and 11.4 mL of deionized water were added to reach a final volume of 20 mL. After boiling this mixture for 30 min, 0.6 mL of sodium citrate solution (50 mg mL^{-1}) was rapidly introduced under vigorous stirring and kept boiling for 2 min. The solution color changed from yellow to ruby red. Then, the suspension was cooled and diluted to 100 mL for further uses.

2.3. Preparation of PVA and LYS blend solution

The polymer mixture was prepared by dissolving 1 g of PVA in 10 mL of deionized water at 80°C for 4 hours. After cooling, different amounts of lysine were added to the PVA solution to achieve 10, 20 and 30 %wt. referred to the weight of PVA (Table 1). Citric acid (CA), used as in-situ crosslinking agent, was added to all blends in a percentage of 15% of

149 the total polymer weight. Prior to use for electrospinning, the mixture was stirred for 1 h to
150 obtain a homogeneous solution.
151 Pure PVA-CA fibers were also prepared in the same way, without adding lysine to the
152 mixture.
153

Tab. 1 Prepared polymer solutions

Sample Name	Amount of lysine in PVA blend (wt %)	Amount citric acid (wt %) **
PVA-CA*	0	15
PVA-LYS 10	10	
PVA-LYS 20	20	
PVA-LYS 30	30	

154 *PVA-CA: PVA-Citric Acid, **Amount of citric acid is 15 % of total polymer weight

155 2.4. Fabrication of PVA-LYS fibers
156 PVA-LYS fibers were prepared by electrospinning. The setup is composed of a high-voltage
157 power supply, a syringe pump, and a stainless steel collector. The electrospinning process
158 was performed using 30 kV field strength, 15 cm tip-to-collector distance and 0.9 mL min^{-1}
159 flow rate. After electrospinning, the fibers were cured by thermal treatment at 180°C for 30
160 min.
161 2.5. Characterization
162 A Malvern Zetasizer Nano - ZS was used to measure the surface charge of AuNPs. HR-TEM
163 micrographs of AuNPs were obtained using a JEOL JEM 3010 instrument (300 kV)
164 equipped with LaB_6 filament. A few drops of nanoparticles suspension were placed on a 200
165 mesh carbon-coated copper grids and allowed to dry before analysis. Elemental analysis was
166 conducted by a Thermo Fisher FlashEA 1112 Series elemental analyzer. Fibers morphology

was characterized by Zeiss EVO 50 scanning electron micrograph, operating at 10 kV accelerating voltage. The samples were first coated with gold using a Baltec SCD 050 sputter coater for 40 seconds at 60 mA. FTIR spectra were obtained using a Perkin Elmer instrument (Spectrum 100) in attenuated total reflectance (ATR) mode. The spectra were recorded in the range from 650 to 4000 cm^{-1}, at 4 cm^{-1} resolution and 8 scans/spectrum, using a DTGS detector. Thermogravimetric analysis was performed on a TA instrument SDT Q600, under a nitrogen gas flow of 100 ml min^{-1}. About 10 mg of sample were placed in an alumina pan and heated from 30 to 700°C with a ramp of 10°C min^{-1}.

The pH of zero charge (pH_{pzc}) of PVA-LYS fibers was determined using the following experimental procedure: 30 mg of the material were introduced in six Erlenmeyer flasks containing 10 mL of NaCl (0.01 mol L^{-1}) then the pH was adjusted in the range 2 to 12 with HCl or NaOH (0.1 and 1 mol L^{-1}). The mixtures were maintained under stirring for 24 hours. Finally, the final pH was measured using a Metrohm pHmeter and the pH_{pzc} was determined as the intersection of the curve initial pH versus final pH with the bisector (Faria et al. 2004).

The solubility test of PVA-LYS fibers was carried out by introducing 20 mg of each sample in 5 mL deionized water for 24 hours at room temperature. The soluble fraction was obtained by measuring the weight loss after drying the membranes, using the equation 1:

$$W_{loss}(\%) = \frac{(w_0 - w_1)}{w_0} \times 100 \qquad \text{Eq.1}$$

Where, w_0 is the initial weight (mg) and w_1 is the final weight after drying (mg).

2.6. Batch adsorption experiments

The efficiency of PVA-LYS fibers toward AuNPs removal was evaluated by a batch adsorption study. Different amounts of PVA-LYS fibers were added to 5 mL of AuNPs suspension with a concentration of 0.1 mM. The mixtures were kept under stirring (450 rpm) at room temperature. The residual concentration of AuNPs was determined using a Varian Cary 300 Scan UV-Visible spectrophotometer, by measuring the absorption at 520 nm.

Kinetic studies were conducted at different times, ranging from 30 min to 24 h and for two concentrations of AuNPs: 0.1 mM and 0.25 mM. The effect of pH on nanoparticle adsorption was investigated using an initial concentration of 0.1 mM and 10 mg of fibers. The initial pH was adjusted in the range 5 to 9 using 0.1 M HCl or 0.1 M NaOH.

The removal percentage Y (%) and the adsorption capacity q_e (mg g^{-1}) were calculated according to equations 2 and 3:

$$Y = [(C_0 - C_e)/C_0] \times 100 \quad \text{Eq. 2}$$

$$q_e = (C_0 - C_e) \times V/W \quad \text{Eq. 3}$$

where, C_0 (mg L^{-1}) is the initial concentration, C_e (mg L^{-1}) is the concentration at equilibrium, V (L) is the solution volume and W (g) is the adsorbent amount.

All adsorption experiments were performed in triplicate. The error was estimated as the standard deviation of the three measurements.

2.7. Fibers digestion and analysis by ICP-OES

The presence of gold nanoparticles on PVA-LYS fibers after adsorption has been confirmed through the digestion of dried AuNPs/PVA-LYS fibers, followed by ICP-OES measurements. The sample was digested by a microwave oven (Milestone-MEGA 1200) with a mixture of 3 mL of nitric acid and 1 mL of hydrogen peroxide in 100 mL tetrafluoromethoxyl vessels. The following heating steps were applied consecutively: 5 min at 250 W, 5 min at 400W, 5 min at 600 W, 5 min at 250 W and finally 30 min of ventilation. The resulting solutions were filtered on cellulose filters (Whatman Grade 5) to eliminate the undissolved polymer and diluted to 10 mL with HPW (Milli-Q (Millipore) ultrapure water, resistivity = 18.2 MΩ cm). Au concentration was determined by Inductively Coupled Plasma Optical Emission Spectroscopy, ICP-OES (PerkinElmer, model Optima 7000 DV) equipped by a Teflon Mira Mist nebulizer, a cyclonic spray chamber and an Echelle monochromator. The applied power was 1300 W. Plasma, auxiliary and nebulizer gas flows were 15, 0.2 and

214 0.6 L min^{-1} respectively. The signals were measured in triplicate. Au concentration was
215 measured at 267.595 nm.
216
217
218 2.8. Catalytic performance of AuNPs/PVA-LYS
219 The catalytic performance of AuNPs adsorbed on PVA-Lys fibers was evaluated by the
220 reduction of 4-NP in the presence of $NaBH_4$ as a reducing agent. 30 mg of dried fibers,
221 recovered from the AuNPs adsorption experiment from water, were added to a solution of
222 4-NP (1 mM, 5 mL) and a freshly prepared $NaBH_4$ solution (50 mM, 15 mL) under stirring
223 (Hashimi et al., 2019). The kinetic of the reaction was monitored by the absorbance of
224 nitrophenolate ion at the wavelength 400 nm.
225 The following flowchart summarized the methodology used in this work (Scheme 1).

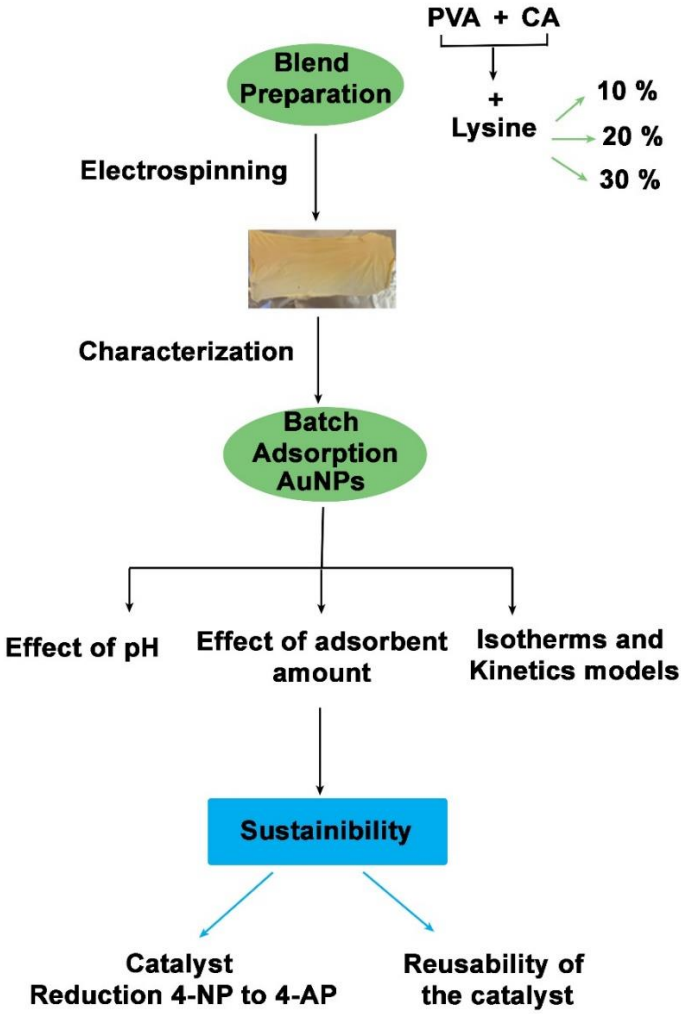

Scheme 1: Flowchart of the methodology

3. Results and discussions

3.1. Characterization

The synthesized AuNPs were characterized using UV-Visible, TEM and Zeta-potential techniques. The UV-Visible spectrum (Fig.2A) shows that the surface plasmon resonance peak occurs at 520 nm, confirming the successful preparation of AuNPs (Hammami et al. 2021). TEM images (Fig.2B) reveal that the nanoparticle shape was uniform and predominantly spherical. Their average size is equal to 13.07 nm ± 2.49 nm (evaluated on a sample of 100 particles, Fig.2C). Zeta potential values were negative over all the pH range as shown in Fig.2D, indicating a good stability of the suspension. These negative values could be associated to the citrate ions adsorbed on the surface of AuNPs (Gicheva et al.

2013). Hence, these results confirm the successful synthesis of stable citrate capped AuNPs with a negatively charged surface.

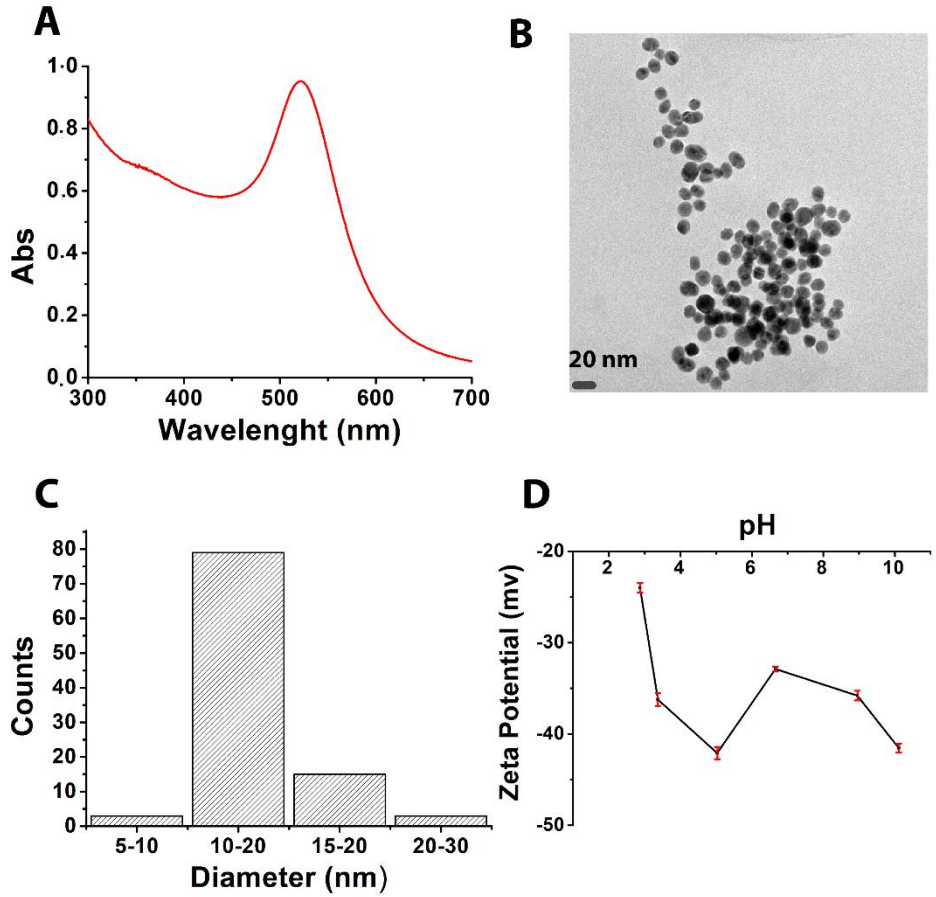

Fig. 2 UV-Visible spectrum of AuNPs (A) TEM image (B) Size distribution of nanoparticles (C) Zeta potential of AuNPs (D)

ATR-FTIR spectra of the three PVA-LYS fibers, PVA-CA fibers, pure PVA and Lysine are shown in Fig.3. In the region between 650 cm^{-1} and 1500 cm^{-1}, the spectrum of pure PVA crosslinked with citric acid presents the characteristic bands at 840, 1092, 1235 and 1420 cm^{-1}, corresponding to C-C (Santos et al. 2014), C-O (Fu et al. 2019), C-C-O stretching (Park et al. 2017) and C-H bending, respectively. The two peaks appearing at 2941 cm^{-1} and 2912 cm^{-1} are related to the symmetric and asymmetric stretching of -CH (Rosli et al. 2022, Fu et al. 2017).

Lysine is usually known to exist in the zwitterionic form in both solid and solution conditions, with the unprotonated carboxyl group ($–COO^-$) and the protonated amino group ($–NH_3^+$). Accordingly, the spectrum of pure lysine shows a distinct absorption at 3356 cm^{-1}, assigned to the asymmetric stretching vibrations of the primary amino group, while the stretching vibration of the protonated amino group gives several broad bands between 2500 and 3200 cm^{-1}. The strong bands at 1571 and 1514 cm^{-1} are attributed to the asymmetric stretching vibration of $-COO^-$ and the bending of $-NH_3^+$ group, respectively (Yao and Huang 2022).

PVA-LYS spectra show: a broad band around 3300 cm^{-1}, assigned to the overlapping of stretching vibrations of O-H and N-H groups (Zhang et al. 2020) and two weak absorption signals at 1595 and 1650 cm^{-1}, attributed to the amidic C=O, resulting from the reaction between the amino groups of lysine and the carboxylic acid groups of CA, as reported by Uranga et al. during the preparation of gelatin fibers (Uranga et al. 2016). Low wavenumber IR signals of these amide groups could be hidden by the intense low-frequency bands of pure PVA crosslinked fibers (Santiago-Castillo et al. 2021). However, a shoulder at 1407 cm^{-1}, typical of lysine, together with the C-N stretching vibration band at 1237 cm^{-1} are also observed.

The ester carbonyl stretching signal of pure crosslinked PVA-CA fibers at 1725 cm^{-1} shifts to 1710 cm^{-1} in the PVA-LYS spectra, confirming the change in the chemical environment due to the presence of lysine in the fibers. This band is assigned to the carbonyl of ester groups, resulting from the crosslinking reaction between the carboxylic group of citric acid and hydroxyl group of PVA. In addition, as the amount of lysine in the material increases, the intensity of this signal decreases, while those at 1595 and 1650 cm^{-1}, attributable to the amide carbonyl groups increase, as if the presence of amino groups of lysine causes a competitive reaction with carboxylic groups of citric acid, hindering the formation of ester

bonds. In conclusion, the ATR-FTIR spectra suggest that lysine can react with the cross-linker (citric acid) through the formation of amide groups, guarantying its grafting onto the PVA fibers.

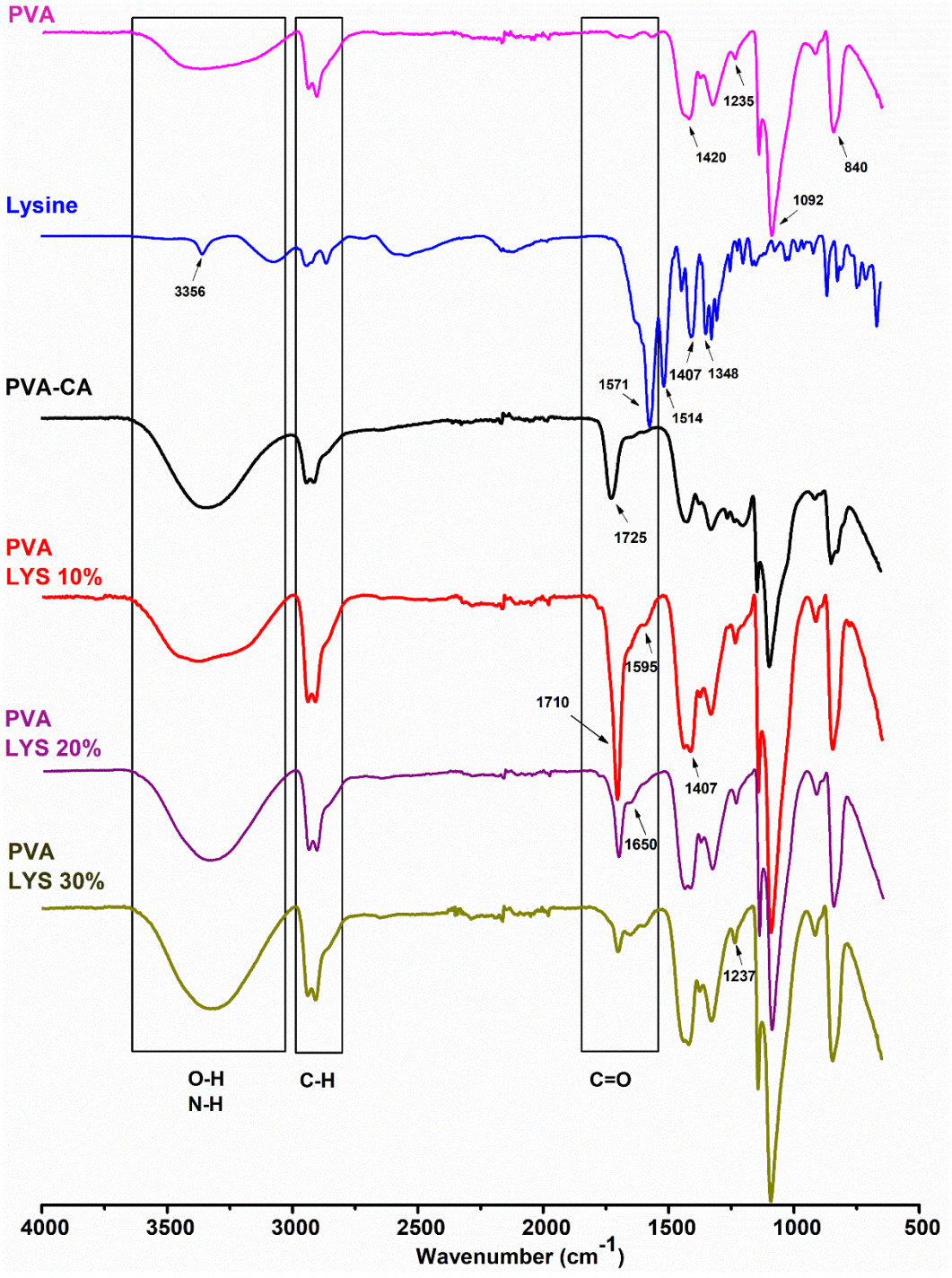

Fig. 3 ATR-FTIR spectra of reference PVA, Lysine, PVA-CA, and PVA-LYS fibers

The thermal stability of PVA-LYS and PVA was studied through their TGA, shown in Fig. 4. The fibers resulted thermally stable up to approximately 200°C. Thermogravimetric

profiles were characterized by a first weight loss step, occurring approximately up to 150°C, which was related to the volatilization of the water adsorbed on the samples or trapped by the hydrophilic hydroxyl groups in the polymer matrix (El-Sayed et al. 2011; Singh et al. 2022). Between 250°C and 500°C a two-step degradation process was observed, as evidenced by the derivative curves (Fig. 4), giving a stable carbon residue at 700°C corresponding approximately to 15% of the initial weight. The first weight loss between 230°C and 350°C might be related to the removal of hydroxyl groups and the formation of polyene, as mentioned by (Tamer et al. 2021). The following weight loss could also be attributed to the decomposition of the PVA main chain and the decomposition of citrate and lysine (Aparecida Toledo Costa et al. 2022; Zhang et al. 2017).

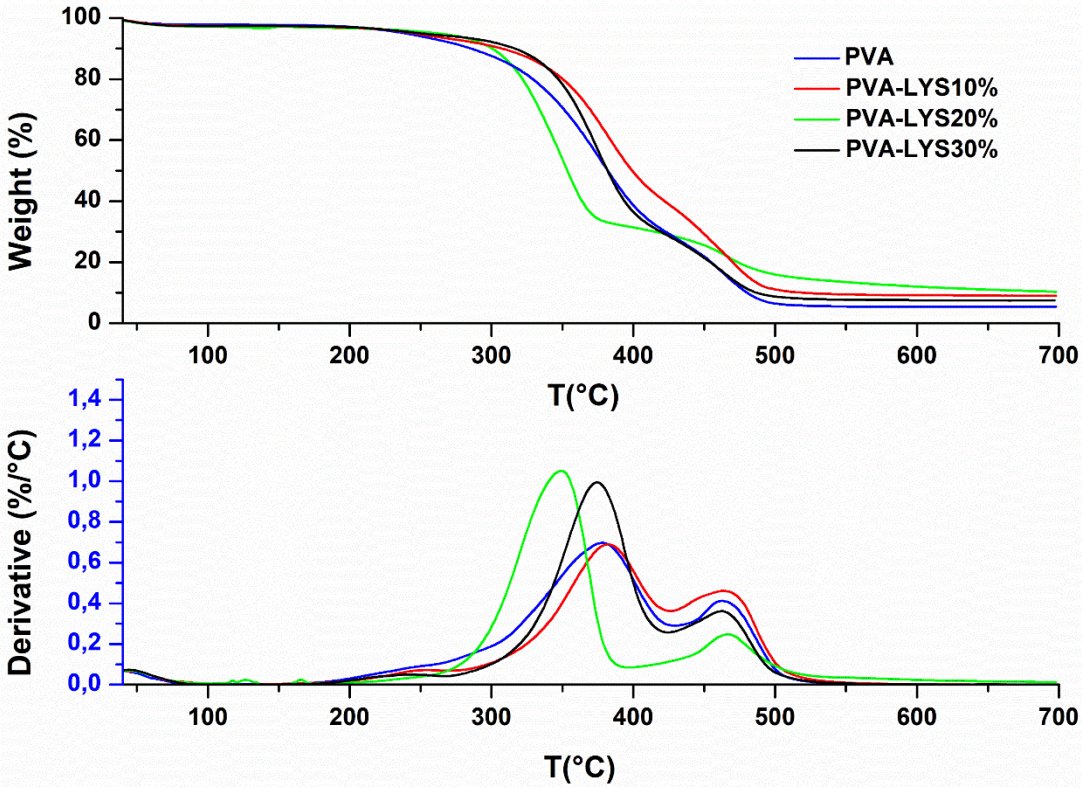

Fig. 4 Thermographs of PVA and PVA-LYS fibers

Fig. 5 presents the nitrogen content in the PVA-LYS fibers as a function of lysine percentage. The amount of nitrogen increases from 1.28% to 3.57% with the loaded concentration of lysine for the unwashed membranes;however, washing the fibers causes a reduction in the

lysine content. The amount of N detected after this step, corresponding to less than 1% for all materials, shows very limited variations from one sample to another. These results indicate that not all the lysine added to the mixture was chemically bonded to the matrix, and moreover that the material reaches a maximum possible loading corresponding to about 0.9%. The solubility test shows that more than 75 wt% of the initial material is unsoluble, as the soluble fractions were 12.5 ± 1.4 wt%, 23.7 ± 4.2 wt% and 27.4 ± 2.6 wt%, for PVA-Lys 10, 20 and 30%, respectively. The observed weight loss can be associated to the uncrosslinked PVA chains and the released lysine after wahing. The results of the elemental analysis and the soluble fractions values proved that the amino acid has been grafted on the PVA, which is accordance with the FTIR adsorption bands of PVA-LYS.

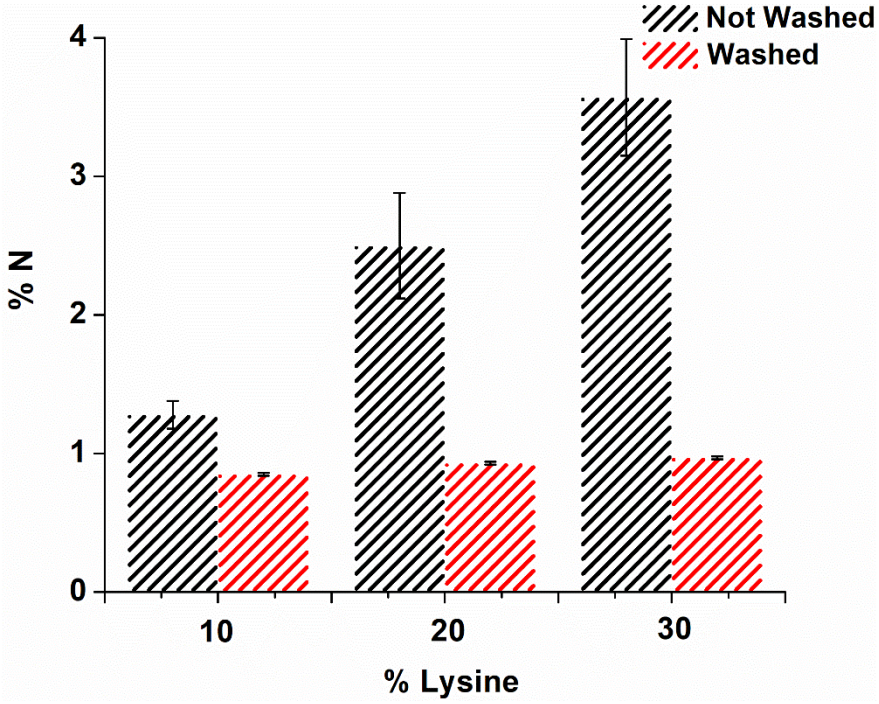

Fig. 5 Nitrogen content in PVA-LYS fibers

The morphological features of the membranes were studied through SEM, as shown in Fig.6. The PVA fibers (Fig. 6A) showed a circular and smooth surface morphology, without any beads formation, and their average diameter was 177 nm ± 25 nm. After the addition of lysine, the morphology of the modified fibers was maintained compared to the PVA fibers.

The diameter and morphology of the PVA-LYS fibers were smooth and uniform along the fiber axis. The average diameter of the PVA-LYS fibers is presented in Table 2. A proportional increase in diameter is observed, with increasing the lysine percentage, explained by the increase in the overall blend concentration (Nezarati et al. 2013). This increase could also result by the interactions between PVA and CA, as well as between PVA and LYS (Zhang et al. 2020).

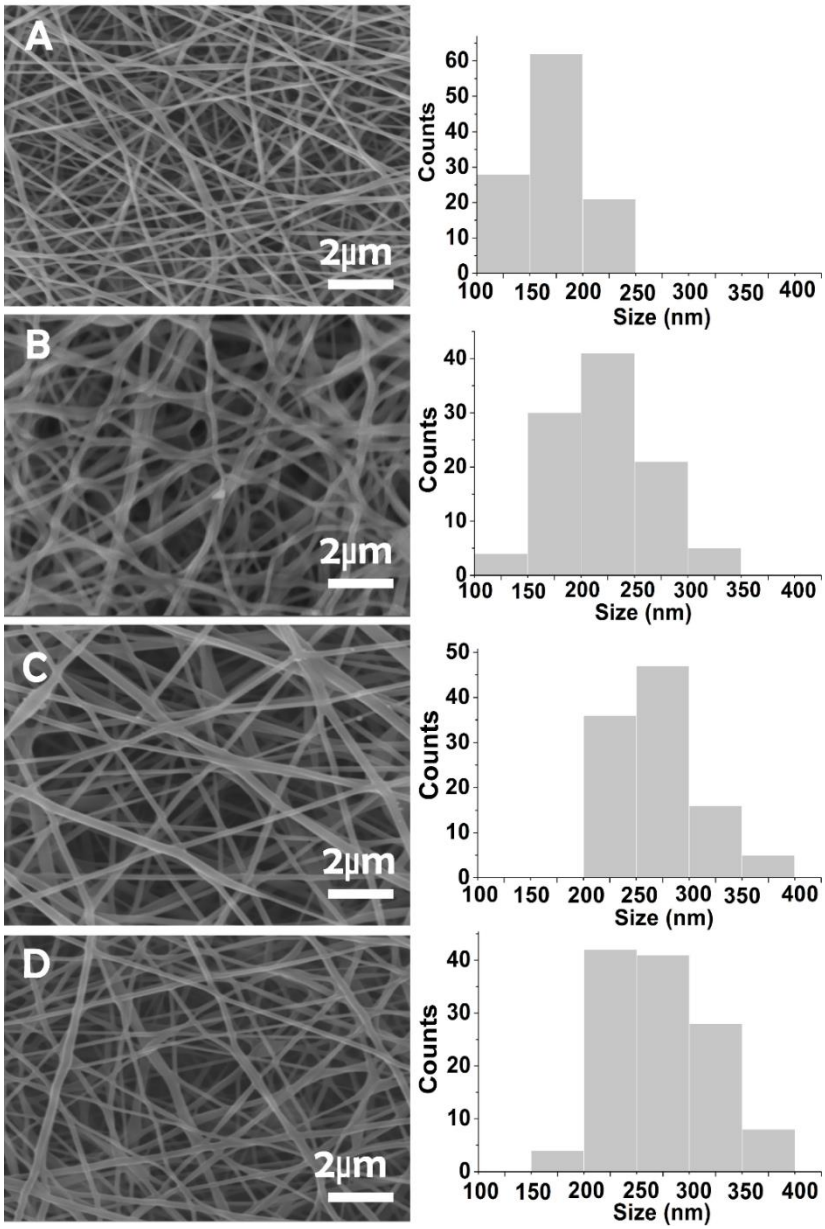

Fig. 6 SEM images and size distribution of PVA (A), PVA-LYS 10% (B), PVA-LYS 20% (C) and PVA-LYS 30% (D) fibers

322

323

Tab. 2 Average diameter of PVA and PVA-LYS fibers

% Lysine	Average Diameter (nm)
0	177 ± 25
10	222 ± 46
20	268 ± 36
30	272 ± 47

324

325 3.2. Efficiency of PVA-LYS fibers in AuNPs extraction

326 The presence of AuNPs on the fibers was first confirmed by the digestion of PVA-LYS
327 fibers after the adsorption experiment. The concentration of Au on the digested fibers,
328 measured by ICP-OES, was equal to 11.31 ± 0.18 mg g^{-1}. After confirming the presence of
329 AuNPs on PVA-LYS fibers, the effect of different parameters, such as pH, amount of fibers
330 and initial AuNPs concentration are investigated in this section. The effect of pH on the
331 nanoparticles adsorption is an important key to understand the interaction mechanisms
332 involved in the adsorption process. The choice of a pH range from 5 to 9 was based on the
333 region where NPs are stably suspended, to avoid their aggregation and consequent
334 precipitation that could affect the results (Li et al. 2014). In all these experiments only,
335 washed fibers were tested. The AuNPs removal percentage decreased with increasing pH, as
336 shown in Fig.7A. A significant improvement in removal efficiency was observed when
337 switching from PVA-LYS 10% to PVA-LYS 30%. The AuNPs adsorption percentage
338 reached 70% at pH 5 for PVA-LYS 30%. The pH effect can be explained in terms of pH_{pzc}
339 of the adsorbent. pH_{pzc} was equal to 4.60, 4.98 and 5.80 for PVA-LYS 10, 20 and 30%,

340 respectively (Fig.7B). The surface of PVA-LYS 30%, and only that, is therefore positively
341 charged when pH is below 5.80. At pH 5, the electrostatic attraction between the positively
342 charged surface fiber of PVA-LYS 30% and the negatively charged citrate capped AuNPs
343 can explain the increase in removal uptake to 65%. However, the electrostatic repulsion
344 between the carboxylate ions present on the fibers and the nanoparticles could explain the
345 decreasing of the removal yield for basic pH. Nevertheless, Fig. 7A shows that the removal
346 percentage for PVA-LYS 30% is around 40%, even for pH above 5, indicating that the
347 electrostatic interaction is not the only mechanism involved in the adsorption process.
348 Selvakannan et al. (2003) demonstrated through NMR investigations that gold nanoparticles
349 can bind to α-amino groups of lysine. Other phenomena involving the matrix need to be
350 hypothesized to explain the results observed for AuNPs removal. In fact, washing causes an
351 important leaching of lysine, as indicated by the N content measurements described in Fig.
352 5. After washing, all samples contain almost the same amount of lysine, but lysine and matrix
353 probably interact more intimately in the sample PVA-LYS 20% and 10%, and this
354 interaction could block part of the amino groups of lysine which are no longer available for
355 AuNPs removal.
356

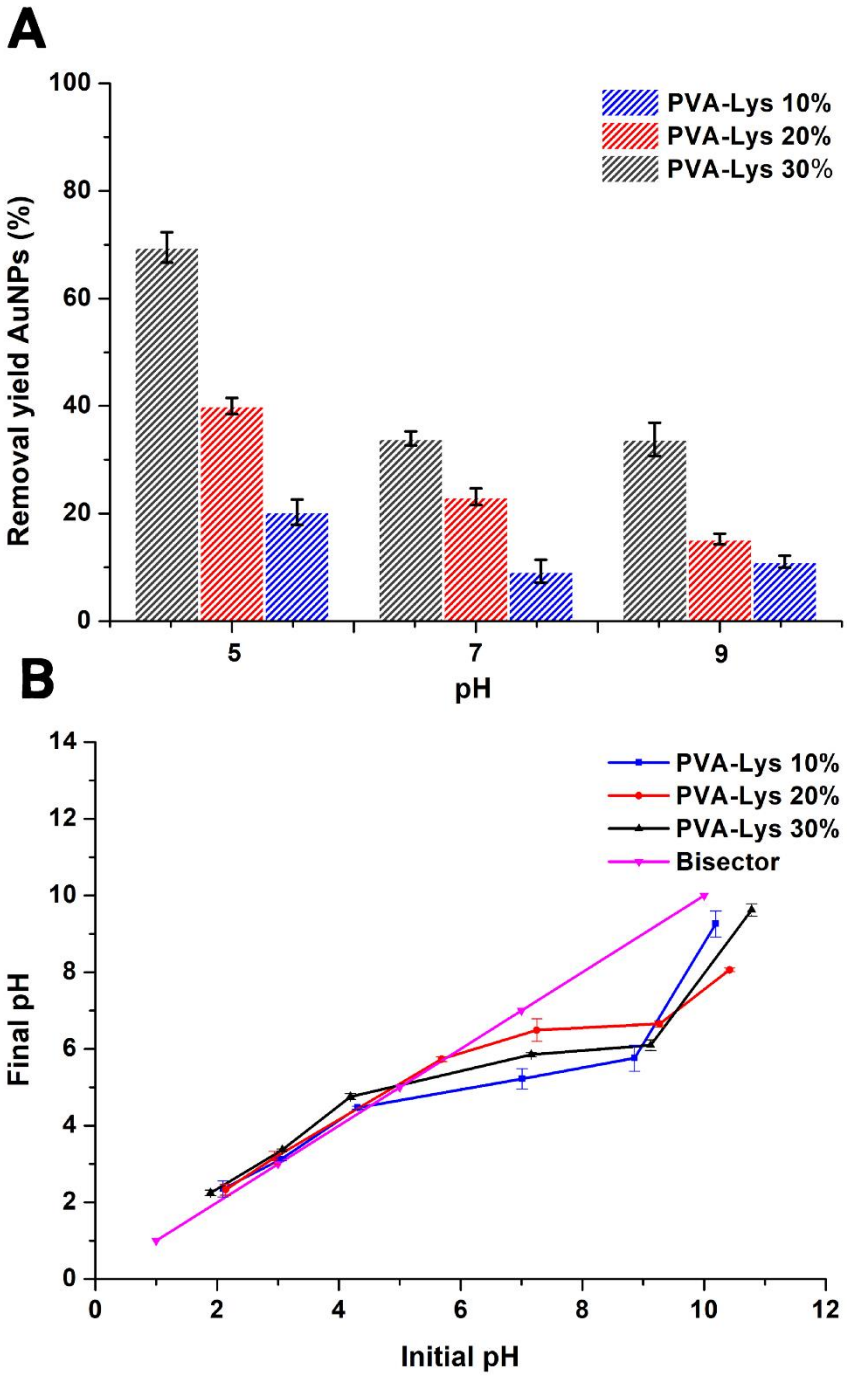

Fig. 7 Effect of pH on AuNPs adsorption for the PVA-LYS fibers (A) Determination of pH_{pzc} of PVA-Lys fibers (B) ([AuNPs] = 0.1 mM, suspension volume = 5 mL, time = 24h, 10 mg fibers)

Different amounts of PVA-LYS fibers were tested to evaluate their effect on AuNPs removal, as shown in Fig. 8. Increasing the fibers amount from 5 to 20 mg produced a higher removal efficiency, reaching 67% for PVA-LYS 30%, due to the presence of a higher

number of functional groups available for interaction with AuNPs (Ahmed et al. 2020). Fibers with 10 and 20 % lysine content showed a slight increase in the removal yield from 5 to 10 mg, then a non-significant enhancement was observed. The next adsorption experiments were performed using the PVA-LYS 30 % fibers and the amount of 20 mg of fibers.

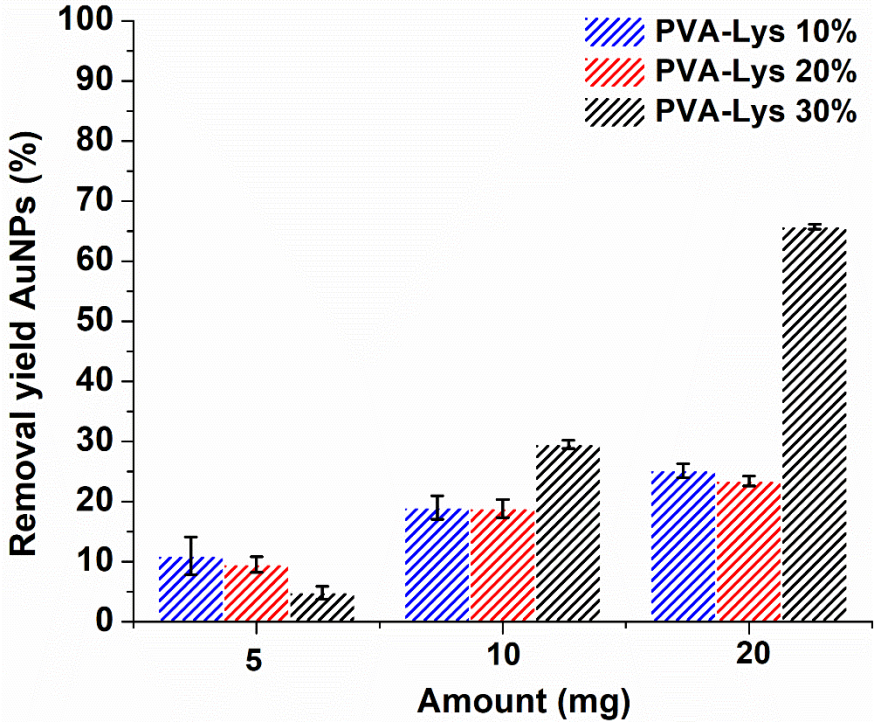

Fig. 8 Effect of PVA-LYS amount ([AuNPs] = 0.25 mM, suspension volume = 5 mL, time = 24h, pH=7)

The kinetics of adsorption of molecules can be determined by their transport toward the surface by diffusion or by interface attachment. The shape and flexibility of the molecules may play a role on the timescale of the kinetic process (Alkafeef and Al-Marri 2016). The kinetic of AuNPs adsorption on PVA-LYS 30% was evaluated at two different AuNPs concentrations (Fig. 9A). AuNPs adsorption reached the equilibrium within 4 hours, with removal yields of 94% and 53% for 0.1 and 0.25 mM, respectively. To better investigate the

adsorption process, the experimental data were fitted with a pseudo first order (Eq.4) (Lagergren et al. 1898) and pseudo second order (Eq.5) (Hamoudi et al. 2018) laws:

$$q_t = q_e\ (1 - \exp(-k_1\, t)) \qquad \text{Eq.4}$$

$$q_t = \frac{k_2\ {q_e}^2\ t}{1 + q_e\, k_2\, t} \qquad \text{Eq.5}$$

where q_t is the adsorption capacity at time t, q_e is the adsorption capacity at the equilibrium (mg g^{-1}), k_1 is the pseudo first order rate constant in min^{-1}, k_2 describes the adsorption rate of the pseudo second order model, expressed in g $mg^{-1}min^{-1}$.

Kinetic parameters are summarized in Table 3 and the non-linear fitting plots are presented in Fig. 9B. The highest values of correlation coefficient (0.997) and lowest Reduced Chi Square (0.015) were obtained in the pseudo first order model, as shown in Table 3, which best represents the interaction mechanism. Also, the calculated values qe_{cal}, determined by the pseudo-first order model, are in accordance with the experimental data: qe_{cal}=7.38 mg g^{-1}, qe_{exp}=7.40 mg g^{-1}, for an initial concentration of 0.25 mM and qe_{cal}=3.68 mg g^{-1}, qe_{exp}=3.69 mg g^{-1}, for an initial concentration of 0.1 mM. This model indicates that the external diffusion and internal diffusion are the rate controlling steps in the adsorption process of gold nanoparticles (Wang and Guo. 2020a).

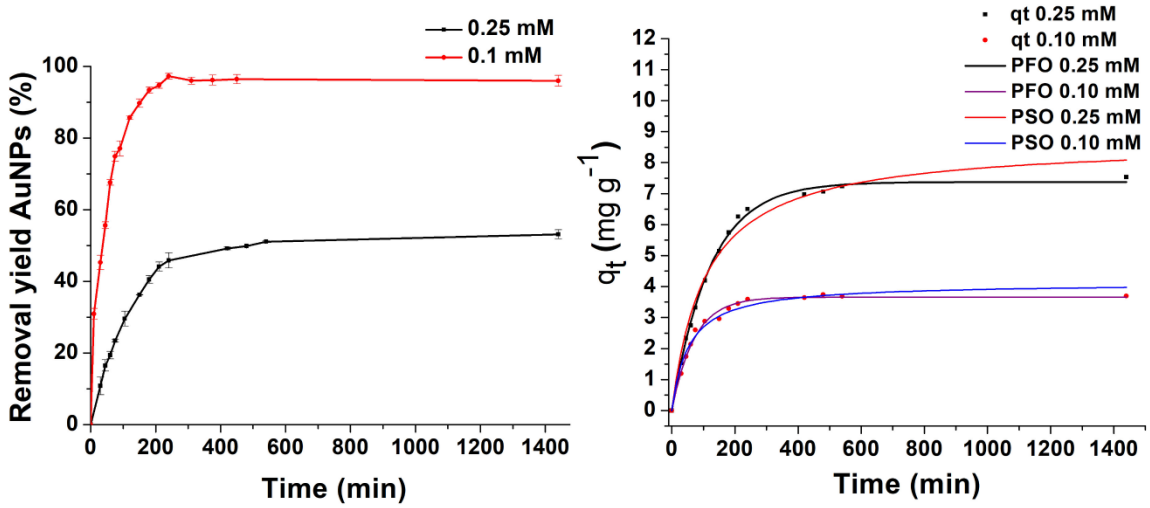

Fig. 9 Effect of contact time for PVA-LYS 30% (A) Kinetic models (B)

([AuNPs] = 0.1 mM and 0.25 mM, 20 mg fibers, suspension volume = 5 mL, pH=7)

Tab.3 Kinetic parameters of Pseudo first order and Pseudo second order models for AuNPs adsorption on PVA-LYS 30%

[AuNPs]	**Pseudo first order**				**Pseudo second order**			
(mM)	qe (mg g^{-1})	k_1 (h^{-1})	χ^2*	r^2	qe (mg g^{-1})	k_2 (g $mg^{-1}h^{-1}$)	χ^2*	r^2
0.10	3.68	0.021	0.022	0.982	4.06	0.008	0.023	0.981
0.25	7.38	0.008	0.015	0.997	8.68	0.001	0.109	0.981

* χ^2: Reduced Chi Square

Adsorption isotherms describe the distribution of the adsorbate between the liquid and solid phase and its interaction with the adsorbent surface (Al-Ghouti and Da'ana 2020).

The experimental data were correlated to the Langmuir and Freundlich models. The Langmuir isotherm model assumes a monolayer adsorption of the molecules (Fu et al. 2021). The equation (Eq.6) is defined as (Mozaffari et al. 2022):

$$q_e = \frac{q_m K_L C_e}{1 + K_L C_e} \qquad \text{Eq. 6}$$

where, q_e (mg g^{-1}) is adsorption capacity at equilibrium, C_e (mg L^{-1}) is equilibrium concentration, K_L is the Langmuir equilibrium constant related to the affinity of binding sites (L g^{-1}) and q_m (mg g^{-1}) represents the maximum adsorption capacity.

Freundlich isotherm model is applied to represent the multi-layer adsorption on heterogeneous surfaces (Wang and Guo 2020b). The non-linear form is described by the following equation (Eq.7):

$$q_e = K_F {C_e}^{1/n} \qquad \text{Eq. 7}$$

where, K_F is the Freundlich constant (L g^{-1}) and n is the heterogeneity factor.

411 The non-linear fitting plots of the two models are represented in Fig. 10 and the
412 corresponding parameters are summarized in Table 4. The values of the correlation
413 coefficient show that the Langmuir model (r^2 = 0.948) fits better the experimental data,
414 indicating a monolayer adsorption onto homogenous surface. According to the Langmuir
415 model, the maximum adsorption capacity of AuNPs is equal to 20.10 mg g^{-1}. Table 5 presents
416 a comparative study between the efficiency of different materials and that of the fibers
417 prepared in this work towards AuNPs removal. This table shows that several adsorbents
418 performed better towards the removal of AuNPs than PVA-Lys fibers. However, others
419 show a lower adsorption capacity, such as cellulosic fibers (Mahanta et al. 2012) and copper
420 oxide (Mallampati et al. 2013). Studies reporting high adsorption capacity for AuNPs
421 (Dhandayuthapani et al. 2014, Kumar et al. 2014) have employed glutaraldehyde as a
422 crosslinker during the fabrication of their materials, however this reagent has shown acute
423 and chronic toxicity, genotoxicity, developmental toxicity, and carcinogenicity (Oh et al.
424 2022). In this work, citric acid has been used as an inexpensive and non-toxic crosslinking
425 agent, to overcome the intrinsic toxicity of the glutaraldehyde (Salihu et al. 2021). It is also
426 important to mention that the use of synthetic polymers like PVA (Zhang et al. 2019, Zhang
427 et al. 2021) and PA-12 (poly-amide) (Aldahash et al. 2022) have demonstrated an interesting
428 perspective and potential in pollutants removal for water.
429 Furthermore, the concentrations of nanoparticles in water are in the range of ppb. The
430 estimated concentration of AgNPs in U.S. surface water is around 10 µg L^{-1} (Conde-
431 González et al. 2016). To extract these low amounts of nanoparticles, a green and eco-
432 friendly material with medium adsorption capacity may be more convenient than an
433 adsorbent showing a high removal efficiency but prepared with toxic reagents.
434

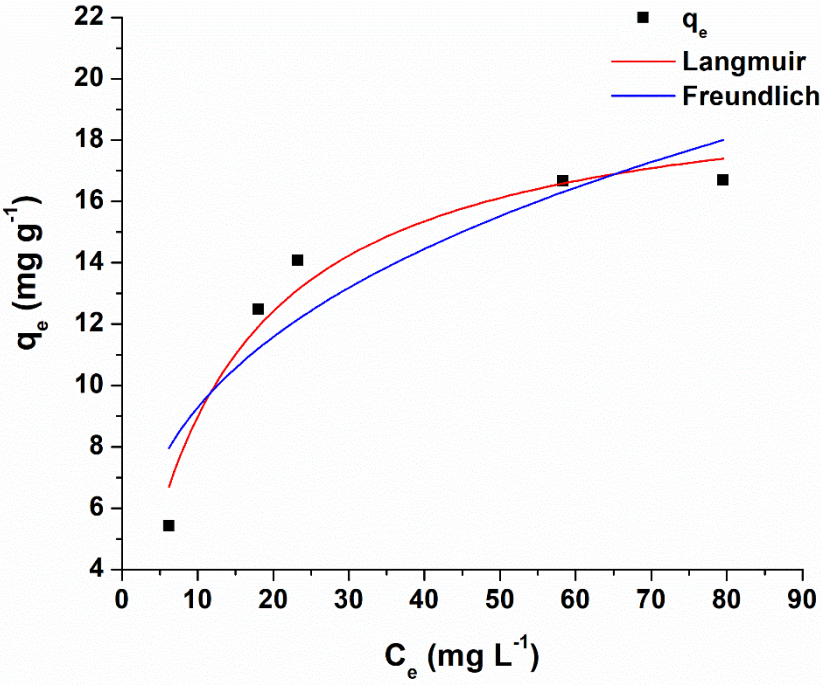

Fig. 10 Isotherms of AuNPs adsorption on PVA-LYS 30%

Tab. 4 Parameters of Langmuir and Freundlich models for AuNPs adsorption on PVA-LYS fibers

	Langmuir model			Freundlich model		
	q_m (mg g^{-1})	K_L (L g^{-1})	r^2	K_F (L g^{-1})	n	r^2
AuNPs	20.105	0.081	0.948	4.449	3.131	0.788

Tab. 5 Maximum AuNPs adsorption capacity (mg g^{-1}) of some adsorbents reported in the literature compared with PVA-LYS fibers

Adsorbent	Q_{max} (mg g^{-1})	Ref
Cellulosic fibers	13.1	(Mahanta et al. 2012)
Biomimetic metal oxides	3.4	(Mallampati et al. 2013)
PVA/Gluten hybrid fibers	36.5	(Dhandayuthapani et al. 2014)
Dopamine-PEI chitosan-coated micro-sized carbon fiber aerogels	32.1	(Liu et al. 2017)
Amine functionalized block copolymers	50.0	(Qureshi et al. 2014)
Functionalized Carbon Spheres	102	(Kumar et al. 2014)
PVA-LYS fibers	20.10	This work

3.3. Proposed adsorption mechanism of AuNPs

Both FTIR and elemental analysis proved the presence of significant number of functional groups on PVA-LYS fibers, such as −OH, −COOH and −CO−NH−. These polar functional groups are responsible of the adsorption process of AuNPs on PVA-LYS fibers. Based on the literature, adsorption is due to electrostatic interactions between nanoparticles and solid surfaces (Brenner et al. 2012). The pH of zero charge is a critical parameter to define the surface charge of the fibers and understand the electrostatic interactions involved in the adsorption mechanism. PVA-LYS 30% have a pH of zero charge equal to 5.8. Thus, their surface charge was positive at pH below 5 and the electrostatic attraction between protonated amino groups of lysine on the fibers and the negatively charged citrate capped AuNPs explains the increase in nanoparticles removal percentage. Furthermore, the functional groups present on the surface of the fibers can form hydrogen bonds with the carboxylic acid groups of citrate capped AuNPs (Dhandayuthapani et al. 2014). The third mechanism that

can also be involved in the adsorption process is the metal-ligand interactions, as demonstrated by Li et al. 2014. Amino groups are considered as ligand with nitrogen donor atom (Nath et al. 2006). These groups have specific affinity towards metallic nanoparticles and are able to form a coordination bond between gold atoms and functional chemical groups, including atoms with a lone electron pair (Dzhimak et al. 2019).

3.4. Catalytic performance of AuNPs/ PVA-LYS fibers

To evaluate the catalytic activity of the adsorbed nanoparticles, reduction of 4-nitrophenol (4-NP) to 4-aminophenol (4-AP) has been widely used in literature as a model reaction (Li et al. 2019; Kumar et al. 2014; Yin et al. 2020). Nitrophenols are extensively used in industries of pharmaceuticals, production of paper, petrochemical, fungicides, pesticides, insecticides, preservatives, explosives, dyes, leather, and wood (Kassem et al. 2021). They are considered as suspected carcinogens and classified as priority pollutants by the United States Environmental Protection Agency (Lin and Doong. 2014). Despite the electrochemical potential values of 4-NP/4-AP (-0.76 V) and H_3BO_3/BH_4^- (-1.33 V), the reduction process is unfavorable due to the electrostatic repulsion between nitrophenolate and borohydride ions (Neal et al. 2019).

During the reduction experiment, AuNPs/ PVA-LYS fibers were added to the mixture of 4-NP (1 mM) with $NaBH_4$ (50 mM). The reaction was monitored using UV-Visible spectrophotometry. In the absence of catalyst, no change was observed in 4-NP peak intensity after 60 min of reaction (Fig.11 A), indicating that $NaBH_4$ was not able to reduce the 4-NP, as expected. After the addition of AuNPs/PVA-LYS fibers, the absorption peak of 4-NP at 400 nm rapidly decreased and a new peak appeared at 300 nm, corresponding to 4-AP (Fig. 11 B). The reduction process was completed within 60 min. The reduction mechanism was elucidated by Neal et al. (2019): the nitrophenolate ion is adsorbed onto the catalyst surface, where it is reduced to 4-AP by a hydrogen atom derived from BH_4^-. The 4-

AP, once generated, rapidly desorbs from the surface of the catalyst. The conversion of 4-NP to 4-AP follows the pseudo first order kinetic model (Noël et al. 2020). The reaction rate was determined using the plot C_t/C_0 versus time, presented in Fig 12. The correlation coefficient r^2 and rate constant k are equal to 0.997 and 0.027 min^{-1}, respectively, similar to previous data reported in the literature (Neal et al. 2019).

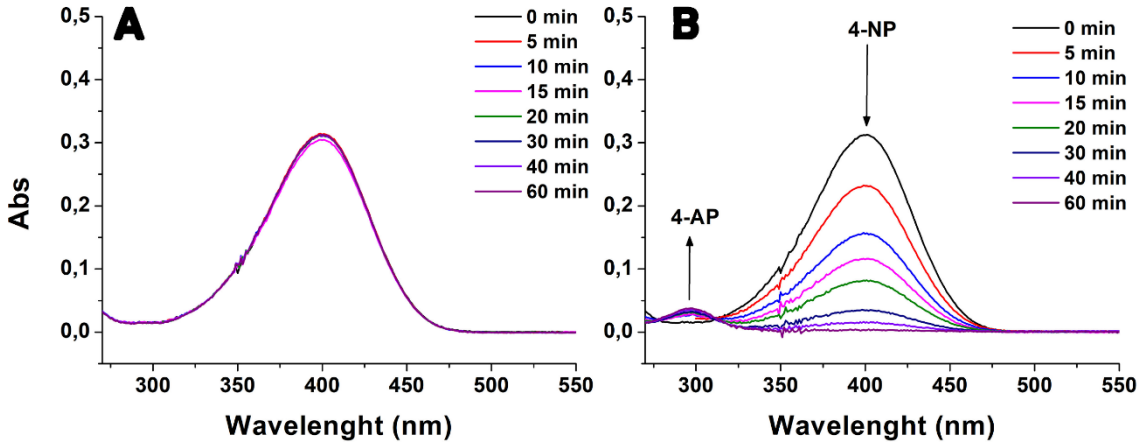

Fig. 11 Time dependent UV-Visible spectra of 4-NP reduction catalyzed without (A) and with AuNPs/PVA-LYS fibers (B)

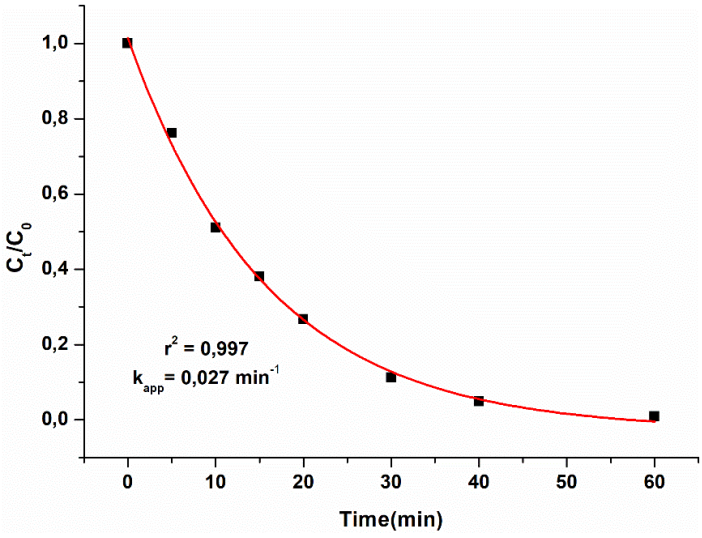

Fig. 12 Kinetic of 4-NP reduction

The reusability of the adsorbed AuNPs on PVA-LYS fibers was tested and the results are presented in Fig. 13. When the reduction was completed, AuNPs/PVA-LYS fibers were collected and added again to a 4-NP solution for the next catalysis cycle. The catalytic

activity was expressed in terms of removal percentage of 4-NP. The reduction process was completed with more than 99% of 4-NP removal during the 5 cycles, indicating the good reusability of this catalyst.

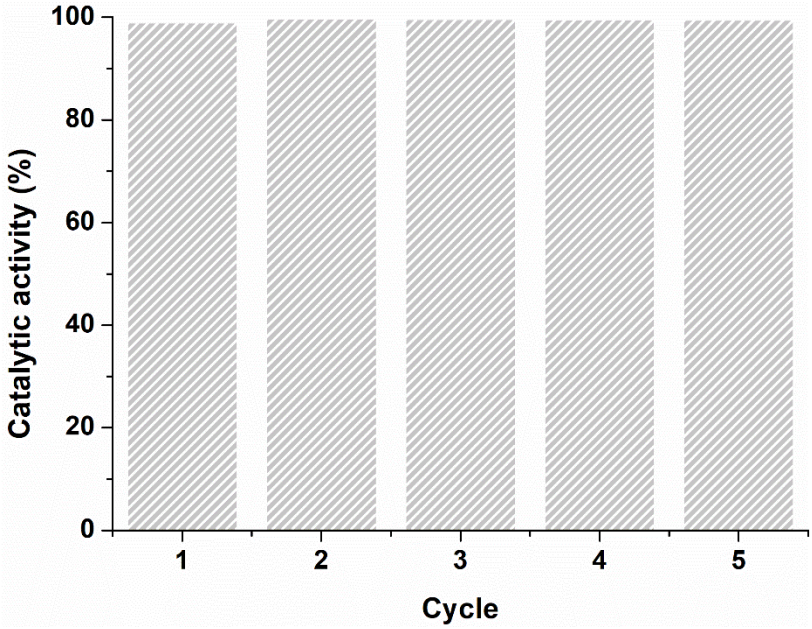

Fig. 13 Reusability of AuNPs/PVA-LYS fibers

3.5. Operational cost of the preparation of PVA-LYS fibers

A cost estimate of the production of these fibers has been elaborated based on the raw materials cost and the energy consumption for the treatment of 1 L of water containing 0.1 mM (19.7 mg L^{-1}) AuNPs. The total cost of raw material was estimated to 1.46 €. In addition, the cost of electricity was determined using the fare for electrical supply per kWh in Italy (0.053 €/kWh). Thus, the total cost for treating 1L of water is equal to 3.05 €. It is important to mention that the real concentration of nanoparticles in water is lower than 1 mg L^{-1} (Islam et al. 2022). This amount of fibers can treat 20 times more than the considered volume of water. There is still a lack of literature dealing with the economic feasibility of this process. (Beck et al. 2017) has found that the annual electrical cost of production of lignin based carbon fibers is around 53,900 $. The scale up of this process is related to the high energy

consumption, which need to be adjusted and produced by renewable resources to reduce the cost.

3.6. Practical applications and perspectives

The prepared PVA-LYS fibers have shown interesting physicochemical properties, such as their smooth morphology without the presence of beads, low diameter size, water stability and presence of different functional groups (hydroxyl, ester, and amide) on their surface. These characteristics can make this adsorption support a promising candidate for the removal of other metallic nanoparticles like AgNPs. Anionic dyes like methylene blue and crystal violet can show electrostatic interactions with the positively charged surface of PVA-LYS fibers at pH lower than 5.8 (pH_{zc}).

To enhance the adsorption capacity of this material and the amount of lysine grafted onto the fibers, other green crosslinking methods can be employed as demonstrated by (Ding et al. 2017).

Conclusion

A green adsorbent was successfully prepared by grafting lysine on biodegradable PVA fibers. The characterization analysis confirms that the amino acid binds covalently to the PVA chain, through amide and ester groups formation during crosslinking in the presence of citric acid. The removal rate reached 65 % at pH equal to 5, by using an adsorbent amount of 20 mg. AuNPs adsorption by PVA-LYS fibers well fitted a pseudo-first-order kinetic and the Langmuir isotherm, with a maximum adsorption capacity of 20.1 mg g^{-1}. The adsorption mechanism of AuNPs involved electrostatic interaction between protonated amino group of lysine and negatively charged AuNPs and metal-ligand interaction between nitrogen atom and gold. Given the increasing demand for green solutions for water remediation, these findings contribute to the development of green and sustainable approaches for nanoparticles removal from aqueous solution, while the reuse of the exhaust material as a catalyst

represents an important added value. Although PVA-LYS fibers are promising green and biodegradable adsorbers, the adsorption capacity of AuNPs nanoparticles should be improved by increasing the amount of nitrogen incorporated in the fibers and remained after washing.

Statements and Declarations

Acknowledgments

The authors acknowledge support from Project CH4.0 under MUR (Italian Ministry for the University) program "Dipartimenti di Eccellenza 2023-2027" (CUP: D13C22003520001).

Funding

This work was financially supported by Compagnia di San Paolo and University of Turin (Bando Ex-Post Anno 2018 and Bando Ex-Post Anno 2020). The fundings of Ricerca Locale 2020 and Ricerca Locale 2021, supplied by University of Turin, are greatly appreciated

Declaration of Competing Interest

The authors declare that they have no competing financial interests or personal relationships that could have appeared to influence the work reported in this paper

Author contributions

All authors contributed to the study conception and design. Eya Ben Khalifa: Conceptualization, Investigation, Methodology, Validation, Writing – original draft, Writing – review and editing. Claudio Cecone: Methodology, Investigation, Validation, Writing – review and editing. Mery Malandrino: Supervision, Project administration, Writing – review & editing. Pierangiola Bracco: Supervision, Project administration, Writing – review & editing. Maria Cristina Paganini: Supervision, Project administration, Funding acquisition, Writing – review & editing. Giuliana Magnacca: Supervision, Project administration, Funding acquisition, Writing – review & editing. All authors read and approved the final manuscript

Data Availability

All data generated or analyzed during this study are included in this article

Ethics declarations

Ethics approval: Not applicable

Consent to participate: All authors participate to this work

Consent for publication: All authors accept to publish this work

References

Ahmed M, Mashkoor F, Nasar A (2020) Development, characterization, and utilization of magnetized orange peel waste as a novel adsorbent for the confiscation of crystal violet dye from aqueous solution. Groundw Sustain Dev 10:100322. https://doi.org/10.1016/j.gsd.2019.100322

Al-Ghouti M A, Da'ana D A (2020) Guidelines for the use and interpretation of adsorption isotherm models: A review. J Hazard Mater 393:122383. https://doi.org/10.1016/j.jhazmat.2020.122383

Alarifi I, Uddin M, Awan A, et al (2020) Synthesis of PAN-nanofibers for the separation of aqueous pollutants and performance of the net-zero energy water treatment plant. Desalination Water Treat 200:90–108. https://doi.org/10.5004/dwt.2020.26064

Aldahash SA, Higgins P, Siddiqui S, Uddin MK (2022) Fabrication of polyamide-12/cement nanocomposite and its testing for different dyes removal from aqueous solution: characterization, adsorption, and regeneration studies. Sci Rep 12:13144. https://doi.org/10.1038/s41598-022-16977-8

Alkafeef SF, Al-Marri SS (2016) Kinetics and isotherms of asphaltene adsorption in narrow pores. Curr Opin Colloid Interface Sci 24:44–51. https://doi.org/10.1016/j.cocis.2016.06.005

587 Amendola V, Pilot R, Frasconi M, Maragò O M, Iatì M A (2017) Surface plasmon resonance
588 in gold nanoparticles: a review. J Phys Condense Matter 29:202017.
589 https://doi.org/10.1088/1361-648X/aa60f3
590 ANSES (2021) https://www.anses.fr/fr/content/evaluation-des-risques-sanitaires-liés-à-la-
591 présence-de-formaldéhyde, Accessed 28-12-2021
592 Aparecida Toledo Costa L, Contino Vianna de Aguiar L, de Souza Gomes, José Bento Brum
593 E F (2022) Characterization of PVA and phenol salt modified tin dioxide cationic
594 membranes. Int J Hydrog Energy 47:7415–7431.
595 https://doi.org/10.1016/j.ijhydene.2021.12.074
596 Beck RJ, Zhao Y, Fong H, Menkhaus TJ (2017) Electrospun lignin carbon nanofiber
597 membranes with large pores for highly efficient adsorptive water treatment applications. J
598 Water Process Eng 16:240–248. https://doi.org/10.1016/j.jwpe.2017.02.002
599 BCC research reports (2021) https://www.bccresearch.com/market-
600 research/nanotechnology/nanotechnology-fuel-cell-research-review.html, Accessed 28-12-
601 2021
602 Brenner T, Paulus M, Schroer MA, et al (2012) Adsorption of nanoparticles at the solid–
603 liquid interface. J Colloid Interface Sci 374:287–290.
604 https://doi.org/10.1016/j.jcis.2012.02.010
605 Cecone C, Hoti G, Zanetti M, Trotta F, Bracco P (2022) Sustainable production of curable
606 maltodextrine-based ecletrospun microfibers. RSC Adv 12:762.
607 https://doi.org/10.1039/D1RA06785K
608 Conde-González JE, Peña-Méndez EM, Rybáková S, et al (2016) Adsorption of silver
609 nanoparticles from aqueous solution on copper-based metal organic frameworks (HKUST-
610 1). Chemosphere 150:659–666. https://doi.org/10.1016/j.chemosphere.2016.02.005

611 Dhandayuthapani B, Mallampati R, Sriramulu D, Fredrick Dsouza R, Valiyaveettil S (2014)
612 PVA/Gluten hybrid nanofibers for removal of nanoparticles from water, ACS Sustain Chem.
613 Eng 2:1014-1021. https://doi.org/10.1021/sc500003k
614 Ding W, Zhou J, Zeng Y, et al (2017) Preparation of oxidized sodium alginate with different
615 molecular weights and its application for crosslinking collagen fiber. Carbohydr Polym
616 157:1650–1656. https://doi.org/10.1016/j.carbpol.2016.11.045
617 Du X, Zhou W, Zhang W, Sun S, Han Y, Tang Y, Shi W, Liu G (2021) Toxicities of three
618 metal oxide nanoparticles to a marine microalga: Impacts on the motility and potential
619 affecting mechanisms. Environ Pollut 290 :118027.
620 https://doi.org/10.1016/j.envpol.2021.118027
621 Dzhimak SS, Malyshko VV, Goryachko AI, et al (2019) ADSORPTION OF SILVER
622 NANOPARTICLES ON MONO- AND POLYFILAMENT FIBERS. Nanotechnologies
623 Russ 14:48–54. https://doi.org/10.1134/S199507801901004X
624 Elkady M, Salama E, Amer WA, et al (2020) Novel eco-friendly electrospun nanomagnetic
625 zinc oxide hybridized PVA/alginate/chitosan nanofibers for enhanced phenol
626 decontamination. Environ Sci Pollut Res 27:43077–43092. https://doi.org/10.1007/s11356-
627 020-10247-8
628 El-Sayed S, Mahmoud K H, Fatah A A, Hassen A (2011) DSC, TGA and dielectric
629 properties of carboxymethyl cellulose/polyvinyl alcohol blends, Physica B Condens Matter
630 406:4068-4076. https://doi.org/10.1016/j.physb.2011.07.050
631 Faria P C C, Órfão J M M, Pereira M F R (2004) Adsorption of anionic and cationic dyes on
632 activated carbons with different surface chemistries. Water Res 18 :2043-2052.
633 https://doi.org/10.1016/j.watres.2004.01.034

Franco R A, Min Y-K, Yang H-M, Lee B-T (2012) On Stabilization of PVPA/PVA Electrospun Nanofiber Membrane and Its Effect on Material Properties and Biocompatibility. J Nanomater 393042. https://doi.org/10.1155/2012/393042.

Fu D, Huang Y, Zhang X, et al (2017) Uncovering potentials of integrated TiO2(B) nanosheets and H2O2 for removal of tetracycline from aqueous solution. J Mol Liq 248:112–120. https://doi.org/10.1016/j.molliq.2017.10.020

Fu D, Kurniawan TA, Avtar R, et al (2021) Recovering heavy metals from electroplating wastewater and their conversion into Zn2Cr-layered double hydroxide (LDH) for pyrophosphate removal from industrial wastewater. Chemosphere 271:129861. https://doi.org/10.1016/j.chemosphere.2021.129861

Fu D, Kurniawan TA, Li H, et al (2019) Applicability of HDPC-supported Cu nanoparticles composite synthesized from anaerobically digested wheat straw for octocrylene degradation in aqueous solutions. Chem Eng J 355:650–660. https://doi.org/10.1016/j.cej.2018.08.188

Gicheva G, Yordanov G (2013) Removal of citrate-coated silver nanoparticles from aqueous dispersions by using activated carbon. Colloids. Surf. A Physicochem Eng Asp 431:51-59. https://doi.org/10.1016/j.colsurfa.2013.04.039

Grieger K, Jones J L, Hansen S F, Hendren C O, Jensen K A, Kuzma A, Baun A (2019) Best practices from nano-risk analysis relevant for other emerging technologies, Nat. Nanotechnol. 14:998-1001. https://doi.org/10.1038/s41565-019-0572-1

Haase A, Rott S, Mantion A, Graf P, Plendl J, Thünemann A F, Meier W P, Taubert A, Luch A, Reiser G (2012) Effects of silver nanoparticles on primary mixed neural cell cultures: uptake, oxidative stress and acute calcium responses. Toxicol Sci 126:457-468. https://doi.org/10.1093/toxsci/kfs003

Hammami I, Alabdallah N M, Aljomaa A, Kamoun M (2021) Gold nanoparticles: Synthesis properties and applications. J K Saud Univ Sci 33:101560. https://doi.org/10.1016/j.jksus.2021.101560

Hamoudi S A, Hamdi B, Brendlé J (2018) Removal of ions Pb^{2+} and Cd^{2+} from aqueous solution by containment geomaterials. in: Dincer I, Ozgur Colpan C, Kizilkan O (ed) Exergetic, Energetic and Environmental Dimensions, Academic Press, 1029-1043

Hashimi A S, Mohd Nohan M A N, Chin S X, Zakaria S, Chia C H (2019) Rapid Catalytic Reduction of 4-Nitrophenol and Clock Reaction of Methylene Blue using Copper Nanowire. Nanomaterials 9:936. https://doi.org/10.3390/nano9070936

Hochella M F et al. (2019) Natural, incidental, and engineered nanomaterials and their impacts on the Earth system. Science 363:6434. https://doi.org/10.1126/science.aau8299

Huang X, El-Sayed M A (2010) Gold nanoparticles: Optical properties and implementations in cancer diagnosis and photothermal therapy. J Adv Res 1:13-28. https://doi.org/10.1016/j.jare.2010.02.002

Islam MA, Dada TK, Parvin MI, et al (2022) Silver ions and silver nanoparticles removal by coffee derived biochar using a continuous fixed-bed adsorption column. J Water Process Eng 48:102935. https://doi.org/10.1016/j.jwpe.2022.102935

Karmakar A, Mallick T, Fouzder Ch, Mukhuty A, Kundu R, Ara Begum N (2019) Antioxidant flavone functionalized fluorescent and biocompatible metal nanoparticles: Exploring their efficacy as cell imaging agents. Nano-Struct Nano-Objects 18:100278. https://doi.org/10.1016/j.nanoso.2019.100278

Kassem A A, Abdelhamid H N, Fouad D M, Ibrahim S A (2021) Catalytic reduction of 4-nitrophenol using copper terephthalate frameworks and CuO@C composite. J Environ Chem Eng 9:104401. https://doi.org/10.1016/j.jece.2020.104401

Kuchur O A, Tsymbal S A, Shestovskaya M V, Serov N S, Dukhinova, M S, Shtil A A, (2020) Metal-derived nanoparticles in tumor theranostics: Potential and limitations. J Inorg Biochem 209:111117. https://doi.org/10.1016/j.jinorgbio.2020.111117

Kumar J, Mallampati R, Adin A, Valiyaveetti S (2014) Functionalized carbon spheres for extraction of nanoparticles and catalyst support in water. ACS Sustain Chem Eng 2:2675-2682. https://doi.org/10.1021/sc5004242

Lagergren S (1898) About the theory of so-called adsorption of soluble substances. Handl 24:1-39

Lapenna A, Dell'Aglio M, Palazzo G, Mallardi A (2020) "Naked" gold nanoparticles as colorimetric reporters for biogenic amine detection. Colloids Surf A Physicochem Eng Asp 600:124903. https://doi.org/10.1016/j.colsurfa.2020.124903

Li C, Li D, Wan G, Xu J, Hou W (2011) Facile synthesis of concentrated gold nanoparticles with low size-distribution in water: temperature and pH controls. Nanoscale Res Lett 6:440. https://doi.org/10.1186/1556-276X-6-440

Li Q, Liu J, Sun X, Xu L (2019) Hierarchically porous melamine-formaldehyde resin microspheres for the removal of nanoparticles and simultaneously as the nanoparticle immobilized carrier force ACS Sustain Chem Eng 7:867-876. https://doi.org/10.1021/acssuschemeng.8b04490

Liguori A, Uranga J, Panzavolta S, Guerrero P, de la Caba K, Focarete M L (2019) Electrospinning of Fish Gelatin Solution Containing Citric Acid: An Environmentally Friendly Approach to Prepare Crosslinked Gelatin Fibers. Materials 12:2808. https://doi.org/10.3390/ma12172808.

Lin F, Doong R (2014) Highly efficient reduction of 4-nitrophenol by heterostructured gold-magnetite nanocatalysts. App Cat A Gen 486:32-41. https://doi.org/10.1016/j.apcata.2014.08.013

706 Liu R L, Mao S, Wang Y, Wang L, Ge Y H, Xu X Y, Fu Q (2017) A mussel-inspired hybrid
707 copolymer adhered to chitosan-coated micro-sized carbon fiber aerogels for highly efficient
708 nanoparticle scavenging, Environ Sci Nano
709 4:2164- 2174. https://doi.org/10.1039/C7EN00615B.
710 Mahanta N, Leong W Y, Valiyaveettil S (2012) Isolation and characterization of cellulose-
711 based nanofibers for nanoparticle extraction from an aqueous environment. J Mater Chem
712 22:1985-1993. https://doi.org/10.1039/C1JM15018A
713 Mallampati R, Valiyaveettil S (2013) Biomimetic metal oxides for the extraction of
714 nanoparticles from water. Nanoscale 5 :3395-3399. https://doi.org/10.1039/c3nr34221b
715 Mansur H S, Sadahira C M, Souza A N, Mansur A A P (2008) FTIR spectroscopy
716 characterization of poly (vinyl alcohol) hydrogel with different hydrolysis degree and
717 chemically crosslinked with glutaraldehyde. Mater Sci Eng C 28:539-548.
718 https://doi.org/10.1016/j.msec.2007.10.088
719 Manuja A, Kumar B, Kumar R, Chhabra D, Ghosh M, Manuja M, Brar B, Pal Y, Tripathi B
720 N, Prasad M (2021) Metal/metal oxide nanoparticles: Toxicity concerns associated with their
721 physical state and remediation for biomedical applications, Toxicol Rep 8:1970-1978.
722 https://doi.org/10.1016/j.toxrep.2021.11.020
723 Mao B H, Chen Z Y, Wang Y J, Yan S J (2018) Silver nanoparticles have lethal and
724 sublethal adverse effects on development and longevity by inducing ROS-mediated stress
725 responses, Sci Rep 8:2445. https://doi.org/10.1038/s41598-018-20728-z
726 Montes-Garcı V, Squillaci M A, Diez-Castellnou M, Khac Ong Q, Stellacci F, Samori P
727 (2021) Chemical sensing with Au and Ag nanoparticles. Chem Soc Rev 50:1269-1304.
728 https://doi.org/10.1039/D0CS01112F.

729 Mozaffari Majd M, Kordzadeh-Kermani V, Ghalandari V, Askari A, Sillanpää M (2022)
730 Adsorption isotherm models: A comprehensive and systematic review (2010-2020). Sci
731 Total Environ 812:151334. https://doi.org/10.1016/j.scitotenv.2021.151334
732 Nath S, Ghosh SK, Kundu S, et al (2006) Is Gold Really Softer than Silver? HSAB Principle
733 Revisited. J Nanoparticle Res 8:111–116. https://doi.org/10.1007/s11051-005-8025-1
734 Neal R D, Inoue Y, Hughes R A, Neretina S (2019) Catalytic reduction of 4-nitrophenol by
735 gold catalysts: the influence of borohydride concentration on the induction time. J Phys
736 Chem C 123:2894-12901. https://doi.org/10.1021/acs.jpcc.9b02396
737 Nezarati R M, Eifert M B, Cosgriff-Hernandez E (2013) Effects of humidity and solution
738 viscosity on electrospun fiber morphology. Tissue Eng Part C Methods 19:810-819.
739 https://doi.org/10.1089/ten.TEC.2012.0671
740 Noël S, Bricout H, Addad A, Sonnendecker C, Zimmermann W, Monflier E, Léger B (2020)
741 Catalytic reduction of 4-nitrophenol with gold nanoparticles stabilized by large-ring
742 cyclodextrins. New J Chem 44:21007-21011.https://doi.org/10.1039/D0NJ03687K
743 Oh H-N, Yoo D, Park S, et al (2022) Developmental neurotoxicity induced by
744 glutaraldehyde in neuron/astrocyte co-cultured cells and zebrafish. Ecotoxicol Environ Saf
745 242:113891. https://doi.org/10.1016/j.ecoenv.2022.113891
746 Omer S, Forgách L, Zelkó R, Sebe I (2021) Scale-up of Electrospinning: Market Overview
747 of Products and Devices for Pharmaceutical and Biomedical Purposes. Pharmaceutics
748 13:286. https://doi.org/doi: 10.3390/pharmaceutics13020286
749 Park J A, Kang J K, Lee S C, Kim S B (2017) Electrospun poly(acrylic acid)/poly(vinyl
750 alcohol) nanofibrous adsorbents for Cu(II) removal from industrial plating wastewater. RSC
751 Adv 7:18075-18084. https://doi.org/10.1039/C7RA01362K

752 Picón D, Torasso N, Baudrit JRV, et al (2022) Bio-inspired membranes for adsorption of
753 arsenic via immobilized L-Cysteine in highly hydrophilic electrospun nanofibers. Chem Eng
754 Res Des 185:108–118. https://doi.org/10.1016/j.cherd.2022.06.042
755 Qureshi Z S, Dsoza R, Mallampati R, Valiyaveettil S (2014) Synthesis of amine-
756 functionalized block copolymers for nanopollutant removal from water. J Appl Polym
757 Sci 131:1366-1373. https://doi.org/: 10.1002/app.40943
758 Rosli N, Nisa Yahya W Z, Hakim Wirzal M D (2022) Crosslinked chitosan/poly(vinyl
759 alcohol) nanofibers functionalized by ionic liquid for heavy metal ions removal. Int J Biol
760 Macromol 195:132-141. https://doi.org/10.1016/j.ijbiomac.2021.12.008
761 Rudakov G. A, Tsiberkin K B, Ponomarev R S, Henner V K, Ziolkowska D A, Jasinski J
762 B, Sumanasekera G (2019) Magnetic properties of transition metal nanoparticles enclosed
763 in carbon nanocages. J Magn Mater 472:34-39. https://doi.org/10.1016/j.jmmm.2018.10.016

764 Salihu R, Abd Razak SI, Ahmad Zawawi N, et al (2021) Citric acid: A green cross-linker of
765 biomaterials for biomedical applications. Eur Polym J 146:110271.
766 https://doi.org/10.1016/j.eurpolymj.2021.110271
767 Santiago-Castillo K, Del Angel-López D, Torres-Huerta A M, Domínguez-Crespo M A,
768 Palma-Ramírez D, Willcock H Brachetti-Sibaja S B (2021) Effect on the processability,
769 structure and mechanical properties of highly dispersed in situ ZnO:CS nanoparticles into
770 PVA electrospun fibers. J Mater Res Technol 11:929-945.
771 https://doi.org/10.1016/j.jmrt.2021.01.049
772 Santos C, Silva C J, Büttel Z, Guimarães R, Pereira S B, Tamagnini P, Zille A (2014)
773 Preparation and characterization of polysaccharides/PVA blend nanofibrous membranes by
774 electrospinning method. Carbohydr Polym 99:584-592.
775 https://doi.org/10.1016/j.carbpol.2013.09.008.

776 Selvakannan P R, Mandal S, Phadtare S, Pasricha R, Sastry M (2003) Capping of gold
777 nanoparticles by the amino acid lysine renders them water-dispersible. Langmuir 19:3545-
778 3549. https://doi.org/10.1021/la026906v
779 Singh S, Ghorai M K, Kar K K (2022) Extraction of unburned carbon from coal fly ash. In
780 Kar K K (ed), Handbook of Fly Ash, Butterworth-Heinemann, 403-449
781 Stagi L, Farris R, Engelbrecht L V, Mocci F, Maria Carbonaro C, Innocenzi P (2022) At the
782 root of l-lysine emission in aqueous solutions, Spectrochim. Acta A Mol. Biomol. Spectrosc.
783 283:121717. https://doi.org/10.1016/j.saa.2022.121717
784 Teixeira M A, Amorim M, Felgueiras H P (2019) Poly(Vinyl Alcohol)-Based Nanofibrous
785 Electrospun Scaffolds for Tissue Engineering Applications. Polymers 12:7.
786 https://doi.org/10.3390/polym12010007.
787 Thakur M, Sharma A, Chandel M, Pathania D (2022) Modern applications and current status
788 of green nanotechnology in environmental industry. In: U Shanker, Ch Mustansar Hussain,
789 M Rani (ed), In Micro and Nano Technologies, Green Functionalized Nanomaterials for
790 Environmental Applications, 259-281
791 Thong C C, Teo D C L, Ng C K (2016) Application of polyvinyl alcohol (PVA) in cement-
792 based composite materials: A review of its engineering properties and microstructure
793 behavior. Constr Build Mater 107:172-180.
794 https://doi.org/10.1016/j.conbuildmat.2015.12.188
795 Uranga J, Leceta I, Etxabide A, Guerrero P, de la Caba K (2016) Cross-linking of fish
796 gelatins to develop sustainable films with enhanced properties. Eur Polym J 78:82-90.
797 https://doi.org/10.1016/j.eurpolymj.2016.03.017.
798 Wang J, Guo X (2020a) Adsorption isotherm models: Classification, physical meaning,
799 application and solving method. Chemosphere 258:127279,
800 https://doi.org/10.1016/j.chemosphere.2020.127279

Wang J, Guoa X (2020b) Adsorption kinetic models: Physical meanings, applications, and solving methods. J Hazard Mater 390:122156. https://doi.org/10.1016/j.jhazmat.2020.122156

Wang H, Wang Y, Li C, Jia L (2022) Fabrication of eco-friendly calcium crosslinked alginate electrospun nanofibres for rapid and efficient removal of Cu(II). Int J Biol Macromol 219:1–10. https://doi.org/10.1016/j.ijbiomac.2022.07.221

Wen Y et al. (2021) Electrospinning as a route to advanced carbon fibre materials for selected low-temperature electrochemical devices: A review. J Energy Chem. 59:492-529. https://doi.org/10.1016/j.jechem.2020.11.014

Yao G, Huang Q (2022) Theoretical and experimental study of the infrared and Raman spectra of L-lysine acetylation. Spectrochim Acta A Mol Biomol Spectrosc 278:121371. https://doi.org/10.1016/j.saa.2022.121371

Yin W, Liu M, Zhao T-L, Qian F-J, Li H, Yao Q-Z, Fu S-Q, Zhou G-T (2020) Removal and recovery of silver nanoparticles by hierarchical mesoporous calcite: Performance, mechanism, and sustainable application. Environ Res 187:109699. https://doi.org/10.1016/j.envres.2020.109699

Zhan F, Yan X, Li J, Sheng F, Li B (2021) Encapsulation of tangeretin in PVA/PAA crosslinking electrospun fibers by emulsion-electrospinning: Morphology characterization, slow-release, and antioxidant activity assessment. Food Chem 337:127763. https://doi.org/10.1016/j.foodchem.2020.127763

Zhang A, Zhang Y, Liu Z, Huang G, Wu L, Fu Y, Wang X, Du Y (2022) Anisotropic gold nanostructures applied to improve solar energy conversion. Applied Materials Today 29101575. https://doi.org/10.1016/j.apmt.2022.101575

824 Zhang Q, Uchaker E, Candelaria S L, Cao G (2013) Nanomaterials for energy conversion
825 and storage. Chem Soc Rev 423127:3171. https://doi.org/10.1039/C3CS00009E
826 Zhang S, Shi Q, Christodoulatos C, Meng X (2019) Lead and cadmium adsorption by
827 electrospun PVA/PAA nanofibers: Batch, spectroscopic, and modeling study, Chemosphere.
828 233:405-413. https://doi.org/10.1016/j.chemosphere.2019.05.190
829 Zhang S, Shi Q, Korfiatis G, Christodoulatos C, Wang H, Meng X (2020) Chromate removal
830 by electrospun PVA/PEI nanofibers: Adsorption, reduction, and effects of co-existing ions.
831 Chem Eng J. 387:124179. https://doi.org/10.1016/j.cej.2020.124179
832 Zhang X, Xie L, Wang X, Shao Z, Kong B (2022) Electrospinning super-assembly of
833 ultrathin fibers from single- to multi-Taylor cone sites. Appl Mater Today 26:1-35.
834 https://doi.org/10.1016/j.apmt.2021.101272
835 Zhang X, Zhang Y, Zhang X, Li S, Huang Y (2017) Nitrogen rich core–shell magnetic
836 mesoporous silica as an effective adsorbent for removal of silver nanoparticles from water.
837 J Hazard Mater 337:1-9. https://doi.org/10.1016/j.jhazmat.2017.04.053
838 Zhang Y, Zhu P C, Edgren D (2010) Crosslinking reaction of poly(vinyl alcohol) with
839 glyoxal. J Polym Res 17:725-730. https://doi.org/10.1007/s10965-009-9362-z